

2016

Optimisation of Anodic Oxidation of Aluminium for Enhanced Adhesion and Corrosion Properties of Sol-gel Coatings.

Michael Whelan

Technological University Dublin, michael.g.whelan@tudublin.ie

Tobin Edmond

University of Limerick, edmond.tobin@ul.ie

John Cassidy

Technological University Dublin, john.cassidy@tudublin.ie

See next page for additional authors

Follow this and additional works at: <https://arrow.tudublin.ie/scschcpsart>

 Part of the [Materials Chemistry Commons](#)

Recommended Citation

Whelan, M. et al. (2016) Optimisation of Anodic Oxidation of Aluminium for Enhanced Adhesion and Corrosion Properties of Sol-gel Coatings, *Journal of The Electrochemical Society*, 163 (5) C1-C8 (2016)
DOI : 10.1149/2.0741605jes

This Article is brought to you for free and open access by the School of Chemical and Pharmaceutical Sciences at ARROW@TU Dublin. It has been accepted for inclusion in Articles by an authorized administrator of ARROW@TU Dublin. For more information, please contact arrow.admin@tudublin.ie, aisling.coyne@tudublin.ie.



This work is licensed under a [Creative Commons Attribution-Noncommercial-Share Alike 4.0 License](#)

Authors

Michael Whelan, Tobin Edmond, John Cassidy, J. Colreavy, and Brendan Duffy



Optimisation of Anodic Oxidation of Aluminium for Enhanced Adhesion and Corrosion Properties of Sol-Gel Coatings

M. Whelan,^{a,z} Edmond Tobin,^b J. Cassidy,^c and B. Duffy^a

^aCentre for Research in Engineering Surface Technology, Focas Institute, Dublin Institute of Technology, Dublin 8, Ireland

^bDepartment of Mechanical, Aeronautical and Biomedical Engineering, University of Limerick, Limerick, Ireland

^cDepartment of Chemical and Pharmaceutical Science, Dublin Institute of Technology, Dublin 8, Ireland

The anodising process for clad and bare AA2024-T3 has been optimised as a surface preparation technique prior to sol-gel coating deposition. The combination of anodised aluminum surfaces and organically functionalised sol-gel chemistry have been investigated to impart elevated corrosion resistance and increased mechanical properties to the aluminum metal. A duplex anodising process has been developed to utilise the natural corrosion resistance properties of sulphuric acid anodising with the adhesion and hosting properties of phosphoric acid anodising. The novel anodising process and sol-gel sealed surfaces have been characterized using field emission scanning electron microscopy, energy dispersive X-ray spectroscopy. Performance of the sol-gel treated anodic layers is evaluated by neutral salt spray testing, electrochemical impedance spectroscopy and rain erosion testing.

© 2016 The Electrochemical Society. [DOI: [10.1149/2.0741605jes](https://doi.org/10.1149/2.0741605jes)] All rights reserved.

Manuscript submitted November 30, 2015; revised manuscript received January 22, 2016. Published 00 0, 2016.

Aluminium is used extensively for lightweight structures such as automotive and aerospace components where the combination of strength and corrosion resistance is essential. Aluminium owes its inherent corrosion resistance to a naturally occurring passive oxide which forms on the metal when exposed to the atmosphere.¹ This oxide is nanometre in thickness which limits the metals performance against extreme mechanical and chemical attack.²

Anodising is a process which increases the thickness of the aluminum oxide through an electrochemical reaction in acidic electrolytes such as sulphuric, phosphoric or oxalic acids.¹ The features and properties of the anodic oxides produced are dependent on many parameters including the aluminum alloy, electrolyte type and anodising conditions (e.g. temperature and current density). The process is commonly used to increase corrosion resistance and adhesion properties of the aluminum surface for a variety of applications.

The anodised aluminum oxide layer is nanoporous in structure with a self assembled, hexagonal array of pores extending from the surface of the oxide to a thin barrier layer at the metal oxide interface. The oxide growth and nanopore formation mechanism is a result of flow of anodic alumina in the barrier layer region due to the combination of growth stresses and field assisted plasticity.³⁻⁵ The stresses that drive the flow of material are due to electrostriction of the oxide layer which is plasticised under the electric field.⁴⁻⁶ The flow of material proceeds from the barrier layer into the pore walls forming Al₂O₃ columns in a self assembled structure.

For anti-corrosion applications sulphuric acid anodising (SAA) is most commonly employed.¹ A significant advantage of SAA anodic layers is the ability of the pores to close by surface hydration resulting in elevated barrier properties. Hydration on the SAA surface proceeds rapidly after anodising and can be accelerated by hydrothermal treatment to achieve increased corrosion protection while also entrapping any applied inhibitors of dyes.⁷ Both natural and hydrothermal induced hydration results in pore blocking near the surface of the anodised layer. Hydration continues naturally over time as the pore closing effects move down the pore channel toward the metal surface.⁸ This continued hydration termed “auto-sealing” results in an increase in the barrier properties of the anodic layers even during exposure to aggressive environments.⁹⁻¹¹ Such a feature is responsible for the excellent long term and accelerated corrosion resistance of sulphuric acid anodised layers on copper free wrought alloys.

In the case of copper containing alloys, the protection properties afforded from anodic layers by sulphuric acid anodising is reduced by the inclusion of Cu rich intermetallics in the metal as well as Cu ions within the oxide network.¹² The presence of Cu as well as the random orientation of the pores leads to difficulties with hydration sealing.¹³

To improve the protection on copper containing alloys, novel anodising processes have been developed including boric-sulphuric (BSAA) and tartaric-sulphuric (TSAA) acid anodising for corrosion and adhesive bonding applications. TSAA in particular offers significant advantages over thin film SAA due to the Cu chelating ability of the tartrate ions which increases the barrier properties of the formed layers.¹⁴

Despite the development of novel anodising treatments for copper rich aluminum alloys, the corrosion protection afforded by the anodic layers is limited. To fully protect the aluminum metal the development of novel sealing technologies is required. Sol-gel materials have been extensively studied for corrosion control replacements for Cr(VI) based conversion coatings and are currently being investigated as potential sealing technologies for anodised aluminum.⁹ The sol-gel process can be used to form nanostructured inorganic films (typically 200 nm to 10 μm in overall thickness) that can be tailored to be more resistant than metals to oxidation, corrosion, erosion and wear while also possessing good thermal and electrical properties.¹⁵⁻¹⁷ The chemistry of the sol-gel process is well known¹⁸⁻²⁰ with excellent reviews²¹⁻²³ and books²⁴ available. The most common sol-gel materials used as coatings are based on organically modified silicates (ormosils), which are formed by the hydrolysis and condensation of alkoxide precursors.²⁵

Sol-gel coatings can potentially be tailored to act as sealing agents for anodised aluminum. There are however some inherent problems associated with the combination of sol-gel chemistry and sulphuric acid anodised aluminum layers. Migration of sol-gel materials into the aluminum oxide pores can be limited.²⁶ Furthermore the presence of sol-gel material in the pores of the anodic layers has shown to postpone or fully inhibit the natural hydration of the anodic layers. For the deposition of sol-gel materials on anodic layers it is essential to achieve encapsulation into the porous oxide matrix. This ensures that the hardness and abrasion resistance properties of the anodised surface are afforded to the sol-gel network. It has been reported that sol-gel coatings applied on TSAA anodised aluminum delaminate from the oxide surface after extended corrosion testing.²⁷ If encapsulation is achieved it is critical that the presence of the sol-gel sealer does not affect the hydration and auto-sealing mechanisms of the anodic layers.

For adhesion applications where increased corrosion resistance is not a factor, phosphoric acid anodising (PAA) is also a commonly utilised.¹ The large pore diameters as well as the slow hydration rate of the PAA oxide makes it ideal as an intermediate treatment between the aluminum metal and any applied coatings or adhesives. Unlike the SAA process, PAA treatment imparts limited additional protection to the aluminum surface as hydration induced sealing is not possible, which limits its use in anti-corrosion applications. Recently PAA has been utilised as a successful encapsulation matrix for sol-gel coatings⁹ however protection properties are limited due to the absence

^zE-mail: michael.g.whelan@dit.ie

of significant oxide hydration. In order to achieve both encapsulation of sol-gel materials and unaltered surface hydration, a duplex anodic structure is required. A duplex anodic layer consists of an anodic layer formed from a double anodising process conducted in two different electrolytes. Duplex structures have previously been reported as a result of electro-deoxidising and anodising.²⁸

To optimise the surface preparation of the aluminum surface, a novel anodising process was developed to produce duplex anodic structures on the surface of aluminum alloys. The process was developed to overcome the limitations between forming voltage for the PAA and SAA treatments so that the parameters of each step could be chosen independently. In this way the PAA layer can be tailored to achieve optimum sol-gel encapsulation while the SAA can be used without sol-gel penetration into the pores therefore not affecting the oxide layer hydration. The duplex anodic structure has been utilised for sol-gel deposition however it can be used for any applications requiring combined corrosion resistance of SAA layers with the adhesion properties of PAA.

Experimental

Sol-gel synthesis.—Two sol-gel coatings were synthesised and used as sealers for the anodic layers.

Phenyl functionalised sol-gel.—The silane precursor phenyltriethoxysilane (PhTEOS) (98%) was purchased from VWR International Ltd (Irl). Hydrolysis was conducted under acidic conditions by adding 5.2 ml of 0.04 M HNO₃ to 50.6 ml of silane precursor. 30.6 ml of absolute ethanol was immediately added to the mixture and left to stir for 45 minutes. 13.6 ml of de-ionised water was then added dropwise and the solution was left to stir for 24 h before use. The final molar ratio for the formulation was Silane: Ethanol: Water - 1:2.5:3.5.

Silane-zirconium hybrid sol-gel.—A silane-zirconium sol-gel formulation (Si-Zr) developed previously^{17,29} was also utilised for this work. The silane precursor, 3-(trimethoxysilyl) propylmethacrylate (MAPTMS) (Sigma Aldrich, Irl, Assay (99%) was pre-hydrolysed using 0.01 N HNO₃ for 45 min (solution A). Simultaneously, zirconium (IV) n-propoxide (TPOZ) (Sigma Aldrich, Ireland, Assay ~70% in propanol) was chelated using methacrylic acid (MAAH) (Sigma Aldrich), at a 1:1 molar ratio for 45 minutes (solution B) to form a zirconium complex. Solution A was slowly added to solution B over ten minutes. Following another 45 min, water (pH 7) was added to this mixture. The molar ratio of Si/Zr in the final sol is 4:1 and Si/H₂O is 1:2. After 24 hours of stirring 3,6-Di-2-pyridyl-1,2,4,5-tetrazine (DPTZ) was added as a corrosion inhibitor at a concentration of 0.3% w/v of MAPTMS precursor.

Pre-treatment and anodising.—Unclad AA2024-T3 (Si 0.5%, Fe 0.5%, Cu 0.8-4.9%, Mg 1.2-1.8%, Mn 0.3-0.9%, Cr 0.1%, Zn 0.25%, Ti 0.15% other 0.15%, Al remainder) aluminum panels (150 mm × 100 mm × 0.6 mm) were sourced from Amari (Irl). The panels were degreased in acetone, etched in Novaclean 104 for 45 secs, rinsed and etched in Novox 302 for 90 seconds. Novaclean and Novox were purchased from Henkel (Ger). Acetone, NaOH, HNO₃, H₂SO₄ and H₃PO₄ were purchased from Sigma Aldrich IRL.

AA2024 clad panels with 40 μm of AA1230 (Si 0.2%, Fe 0.5%, Cu 0.03%, Zn 0.03%, Mn 0.03%, Mg 0.005%, Al remainder) were degreased in acetone, etched in 10% NaOH at 40°C for 50 seconds and rinsed in de-ionised water. The panels were then treated in 50% HNO₃ at room temperature for 90 seconds to remove any intermetallics from the surface prior to anodising.

Anodising solutions were prepared by diluting 98% H₂SO₄ w/v and 95% H₃PO₄ in deionised water to a concentration of 25% w/v and 10% w/v respectively. Three anodising procedures were conducted as follows:

1. Phosphoric Acid Anodising (PAA) – 60 min phosphoric acid anodising at constant 40 V.

- Sulphuric Acid Anodising (SAA) - 20 min sulphuric acid anodising at 1.5 A/dm² of aluminum surface area.
- Duplex Anodising (DA) - PAA process was conducted as per procedure 1). At the end of the PAA cycle the anodising current was immediately reduced to half of its steady state value. As a result the anodising potential gradually decreased. Once the anodising voltage decreased to 10 V the power was turned off. The surfaces were then rinsed in de-ionised water for 10 min to remove any residual electrolyte from the pores. The parts were then immersed in the sulphuric acid electrolyte. AA2024-T3 and Clad AA2024-T3 were anodised for 5 and 2 min respectively at 1.5 A/dm² of aluminum surface area.

All anodised samples were rinsed for 20 min in de-ionised water and air dried prior to sol-gel application and testing.

Sealing in sol gel.—For the PAA and SAA surfaces the sol-gel solution was applied immediately after rinsing and drying by a dip coating process. The DA surface was hydrothermally sealed in de-ionised water at 95°C ± 5 for 5 min prior to sol-gel dip coating. In all cases the dip cycle consisted of a 20 minute immersion step in the sol-gel solution following withdrawal at a rate of 10 mm.min⁻¹. The panels were then cured in an oven at 110°C for 16 hours. Hydrothermally sealed (HTS) equivalents of the DA and SAA layers were also produced for comparison.

Electron microscopy.—The anodised films were analyzed by electron microscopy using a Hitachi SU 70 Field Emission Scanning Electron Microscope (FESEM). Anodic film cross sections were prepared by bending the aluminum sample over 180° to induce micro-cracks in the oxide layer. The cross section of the crack face exhibits the pore structure of the anodic alumina for imaging at 1.5 – 4 keV. For imaging purposes the samples were sputter coated with a 4 nm layer of Pt/Pd using a Cressington 208HR sputter coater.

Dot Map energy dispersive X-ray spectroscopy was conducted using an Oxford instruments INCA X-MAX Energy dispersive X-ray spectrometer attached to the FESEM. Cross sections were prepared by mounting samples in epoxy resin then grinding and polishing to a mirror finish using progressive grades of carbide paper and polished to a 1 μm finish with a diamond solution. The polished cross sections were coated with 5 nm of carbon using a Cressington 208C Carbon evaporation coating unit. The Si based sol-gels can be identified by analysing the Si species overlapping with the oxide layer species such as O, P and S.

Electrochemical impedance spectroscopy.—Electrochemical Impedance Spectroscopy (EIS) was conducted on the anodised and sealed AA2024-T3. EIS was carried out using a Solartron SI 1287/1255B system comprising of a frequency analyser and potentiostat operated by CorrView and Z Plot software. A 3.5% NaCl solution was used as the exposure electrolyte and the area of the surface exposed was 4.9 cm². A single area of each system was exposed and evaluated. All measurements were made at the open circuit potential (E_{oc}) with an applied 10 mV sinusoidal perturbation in the frequency range 1 × 10⁶ to 1 × 10⁻¹ Hz (10 points per decade). It was found that frequencies lower than this range produced data points with significant noise. Before measurements were taken the open circuit potential was allowed to stabilise to maximum perturbation of 5 mV. Prior to each experiment a calibrated dummy cell was used to ensure the correct measurement of the system. A calibrated reference electrode, checked against an unused control electrode, was used for each experiment.

Neutral salt spray.—Corrosion resistance testing was conducted in a neutral salt spray environment according to BS EN ISO 9227:2006 with the back and sides of each panel protected with an impermeable electrically insulating tape. The test conditions consisted of a neutral salt fog atmosphere generated from 5 wt% aqueous NaCl solution at 35 ± 1°C. The panels were placed at an angle of 20° (±5) from the vertical to allow the salt spray to settle on the test face. The panels

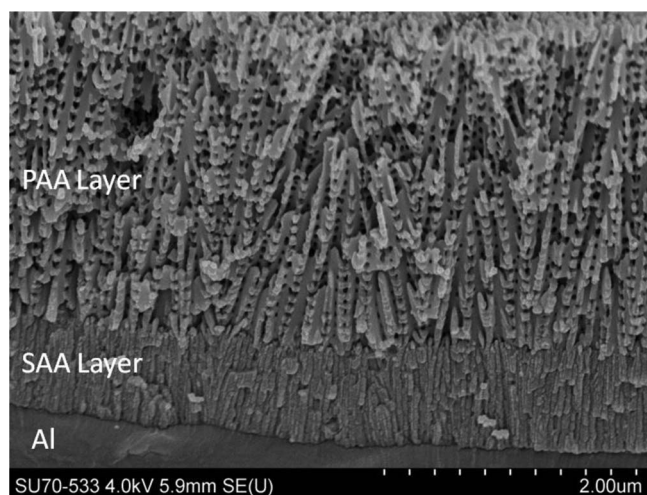


Figure 1. Duplex anodic layer formed on clad AA2024-T3.

239 were exposed to the corrosive conditions for up to 3500 h. A corrosion
240 rating was assigned after each inspection based on the grid method
241 specified in BS EN ISO 12373-19:2001.

242 **Rain erosion.**—To simulate the effect of rain erosion on the an-
243 odised and sol-gel sealed surface, a Whirling Arm Rain Erosion test
244 Rig (WARER) was used. Circular test samples were produced from
245 the anodised and sol-gel treated samples by punch and die. The initial
246 sample mass was recorded. Mass measurements were repeated 3
247 times and taken using an Ohaus Explorer analytical balance with an
248 accuracy of 0.1 mg. Inspection was also carried out for scratches and
249 surface imperfections before testing. An individual test sample was
250 then mounted at the end of the whirling arm. Tests were carried out
251 at 178 ms^{-1} and weight loss was recorded at four test durations; 15,
252 30, 45, and 60 min. The total test duration is based on the length of
253 time the droplet system is active. The rainfall rate was 25 mm/h and
254 was monitored by a flowmeter. A cooling system was used to keep
255 the ambient temperature constant during testing. After each test, the
256 coupons were dried with compressed air and the mass recorded again.

257 Results and Discussion

258 **Anodic layer formation.**—SAA treatment of 2024-T3 and clad
259 2024-T3 alloys have been studied in many publications and the struc-
260 tures and anti-corrosion properties are well documented.^{10,13,14,30-32}
261 DA layers have also been previously reported, however the research
262 to date is limited and the process has not been optimised for sol-
263 gel deposition. The current process produces duplex layers of unique
264 structure as seen in the electron micrograph in Figure 1.

265 The duplex structure consists of a SAA layer approximately $1 \mu\text{m}$
266 in thickness next to the aluminum base metal. This layer exhibits all
267 the natural properties of conventional sulphuric acid anodising such
268 as a small pore diameter as well as surface hydration and auto-sealing.
269 Attached to the surface of the SAA is approximately $2 \mu\text{m}$ of oxide
270 produced from the PAA process. The oxide exhibits a large pore diam-
271 eter with a high level of interporosity. This interconnectivity between
272 pores allows better penetration of liquids into the oxide network as
273 the pressure increase within the pores due to the impinging liquid is
274 easily dissipated.

275 Conventionally the forming voltage of the PAA process is larger
276 than the SAA process. PAA can be conducted up to 200 V while SAA
277 processes generally do not exceed 25 V.¹ The predominant structural
278 effect of the forming voltage is the relative barrier layer thickness with
279 nano-layers formed at approximately 1 nm/V .¹ The barrier layer has
280 been shown to be a significant feature in the electrochemical response
281 of anodised layers.³³ Due to this difference in forming voltage and
282 subsequent barrier layer thickness, burning and rapid dissolution of

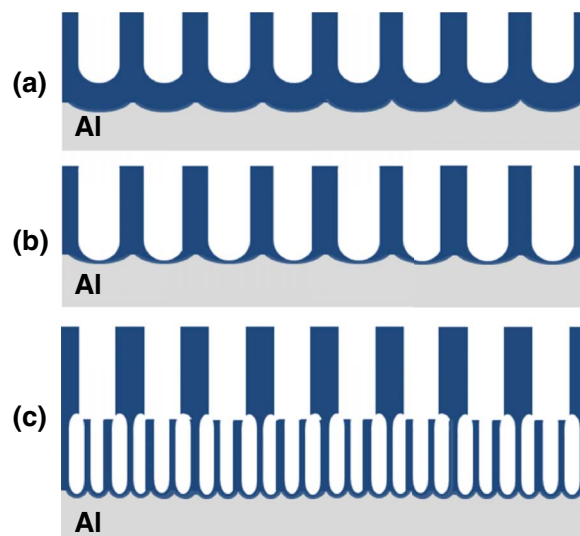


Figure 2. Anodic layer structural change during the duplex anodising cycle.

283 the metal can occur during the SAA cycle due to the insulating effect
284 of the previously formed PAA layer. The critical requirement for the
285 formation of DA layer without burning of the aluminum surfaces is
286 the reduction of the barrier layer thickness of the PAA layer prior to
287 the SAA anodising.

288 After conducting the initial PAA process a porous layer with a
289 relatively thick barrier layer is formed, Figure 2a. The barrier layer
290 formed at the base of the pores is approximately 40 nm in thickness as
291 measured by SEM analysis. It is known that the charge transfer across
292 the barrier is due to ionic conduction of the anodising electrolyte ions
293 as well as Al^{3+} and O^{2-} ions.^{34,35} If the barrier layer thickness is not
294 decreased prior to the SAA process, the application of the second
295 lower steady state anodising potential is not sufficient to allow ionic
296 transfer across the barrier layer. Rather than distributing uniformly
297 across the metal surface, the current will conduct through the point of
298 least resistance. It was found that the process of in-situ electrochemical
299 thinning of the barrier layer (Figure 2b) prior to the second anodising
300 process is critical to prevent burning and dissolution of the metal
301 surface due to large build up of current density at weak spots in the
302 first anodic layer.

303 Barrier layer thinning (BLT) utilises the self regulating nature of
304 the anodising process.³⁶ By rapidly limiting the current at the end
305 of the PAA process to half of the steady state anodising current, the
306 voltage will gradually decrease from the set 40 V to a lower value.
307 During this decrease in voltage, the self regulating characteristic of the
308 anodising process results in a corresponding thinning of the barrier
309 layer Figure 2b. Once a second steady state anodising voltage is
310 reached, the anodising current can again be halved which results in
311 a further voltage drop and continued barrier layer thinning. This step
312 can be further repeated and by sequentially limiting the current in
313 this way a final steady state voltage of the first anodising process
314 can be lowered below the initial anodising voltage of the second
315 anodising process. The results of a BLT process to 10 V and 2 V
316 can be seen in FESEM images in Figure 3. By lowering the forming
317 voltage to 2 V it can be seen that the barrier layer is almost completely
318 removed. Complete removal of the barrier may however compromise
319 the interfacial adhesion between the anodised layers. Barrier layer
320 thinning to a forming voltage of 10 V is sufficient to allow the second
321 anodising process to proceed and in the present study a single current
322 limiting step was required.

323 Once the BLT PAA anodised aluminum is immersed in the SAA
324 electrolyte and a potential above 10 V is applied, ionic conduction
325 across the barrier layer will occur. This results in a thickening of
326 the barrier layer and SAA layer pore nucleation initiates. The SAA
327 layer growth then proceeds uninhibited, Figure 2c. The use of an

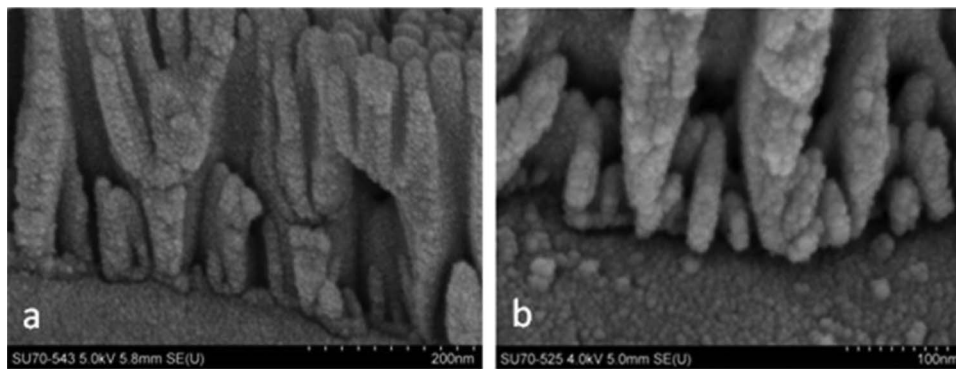


Figure 3. Effect of barrier layer thinning to 10 V (left) and 2 V (right).

intermediate BLT step between the first and second anodising processes allows the parameters for each treatment to be chosen independently. This allows a great deal of flexibility in the layer thickness, pore features and chemical nature of the possible duplex structures that can be formed.

Sol-gel penetration.—There are many factors that can determine if the sol-gel treatment penetrates the porous anodic layers. PAA layers offer the best possibility of penetration due to the large pore diameter, however if the particle size is sufficiently small the sol-gel colloids can also migrate into the SAA layers. In order to determine the penetration properties of the sol-gel on each anodic finish, EDX dot map analysis was used to plot the Si and Al distributions. Figure 4 exhibits the dot maps for the PhTEOS and Si-Zr sol-gel sealed SAA, PAA and DA films on unclad AA2024. The individual layer thicknesses differ from Figure 1, as the alloy is unclad AA2024 as opposed to the clad version in Figure 1.

The PhTEOS exhibits penetration into all surfaces and previous research has shown that the particle size is sufficiently small to allow penetration.⁹ On the SAA layer, which contains the smallest pore diameter, it is clear that the PhTEOS sealer has significant penetration into the oxide with Si intensity deteriorating rapidly at approximately 75% of the oxide thickness. The PAA is known to act as an excellent

host for sol-gel materials⁹ and penetration can be seen again throughout the layer. For the DA layer penetration occurs in the PAA upper layer without evidence of any migration into the SAA base layer probably due to the forced hydration and pore closing between the PAA and SAA layers. In the case of the Si-Zr sol-gel, limited penetration into SAA network occurs. A surface coating only can be distinguished from Figure 4. Similarly to the PhTEOS, the Si-Zr sol-gel penetrates the PAA networks of both the single and duplex anodised layers.

Electrochemical impedance spectroscopy.—EIS analysis was conducted on the un-clad 2024-T3 as the electrochemical response is from the copper rich base metal which is more susceptible to corrosion than the clad material.

The impedance and phase shift spectra for the SAA anodisation with sealers, HTS, PhTEOS and Si-Zr, can be seen in Figure 5. The HTS sealed SAA layer exhibits a characteristic single time constant response. Limited hydration sealing of the pores is detected which is consistent with previous work.⁹ Both sol-gel sealers display increased impedance values, for all frequencies, indicating increased barrier properties of the sol-gel sealers compared to the HTS equivalent. The SAA PhTEOS system displayed a single time constant response indicating that the contributions from the sol-gel sealer and the barrier layer cannot be distinguished. From the EDX analysis it is known that

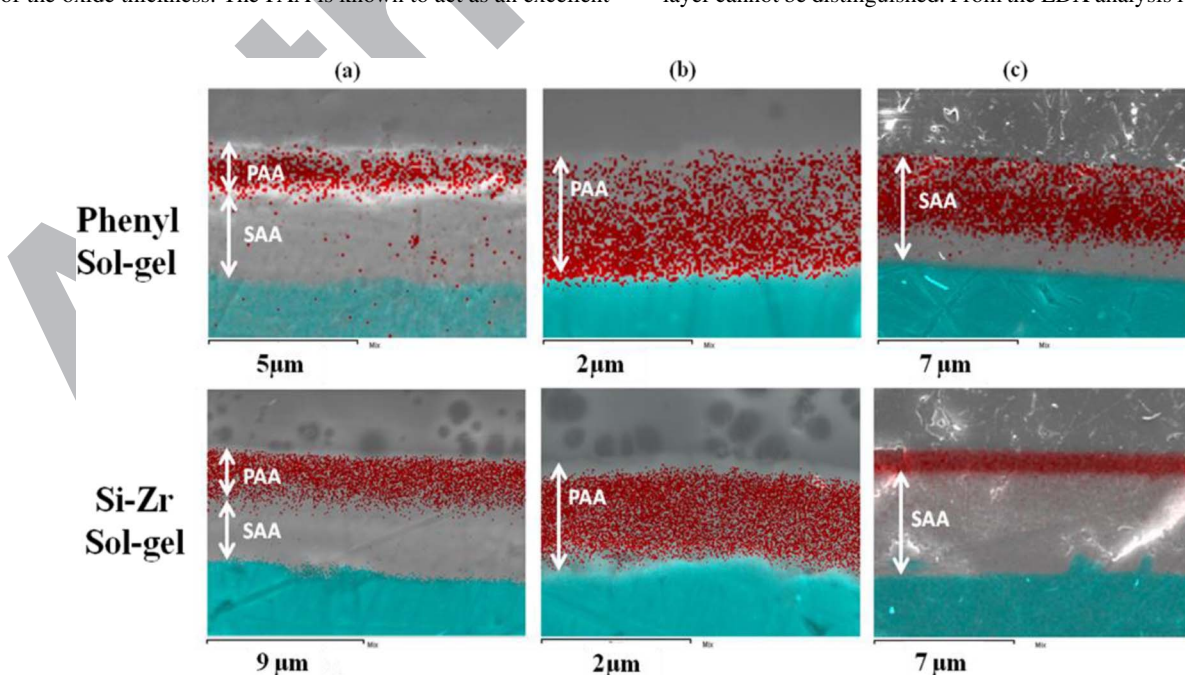


Figure 4. Pore penetration of sol-gel materials (Si (red dots) and Al (blue dots)) into anodised layers on AA2024-T3 (a) DA layer, (b) PAA layer and (c) SAA layer.

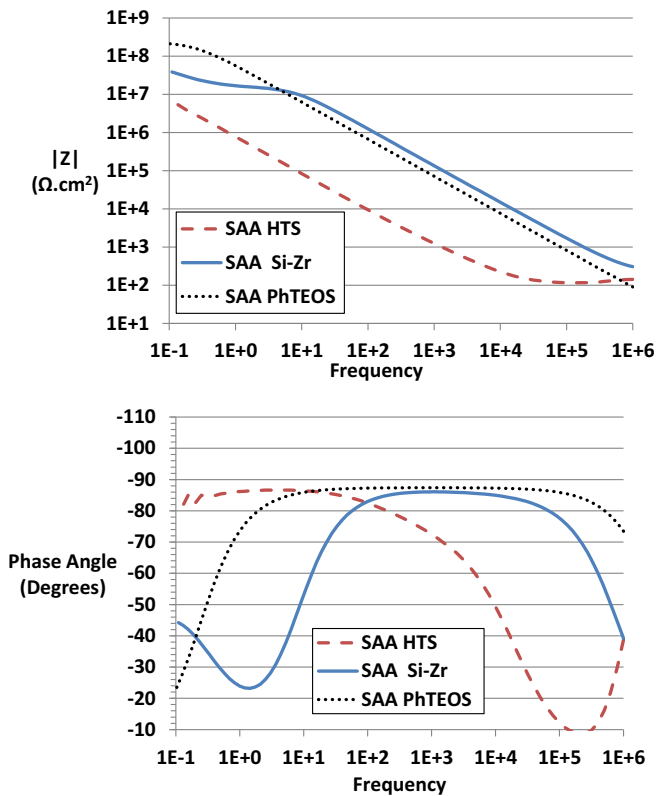


Figure 5. Impedance (top) and phase plot (bottom) for SAA sealed samples.

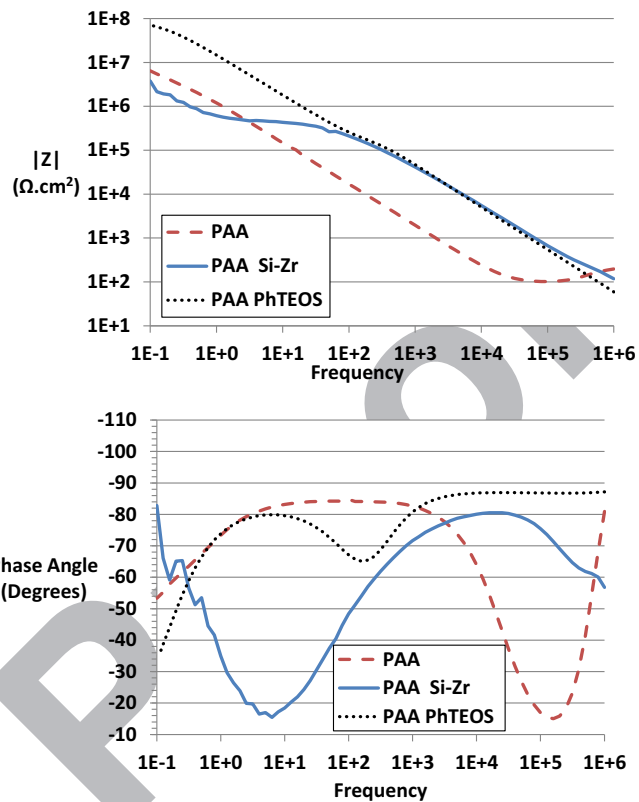


Figure 6. Impedance (top) and phase plot (bottom) for PAA sealed samples.

372 this sealer penetrates the porous network and the EIS response is as
 373 a result of the sol-gel/oxide composite layer. PhTEOS sol-gel sealed
 374 SAA anodic layers have been previously reported on 3003 and have
 375 produced a similar single time constant response.²⁶

376 In contrast the SAA Si-Zr system exhibited a second time constant.
 377 As this sol-gel system acts as a surface coating on the anodic layer, the
 378 impedance response likely comprises the response from the surface
 379 coating and the barrier layer. The effect of the penetration of the
 380 PhTEOS sealer compared to the Si-Zr equivalent can be seen in the low
 381 frequency impedance values (<1 Hz). The PhTEOS system displays
 382 higher impedance values, in this frequency region, due to the presence
 383 of the sol-gel in the pores.

384 The impedance and phase shift spectra for PAA sealed anodic
 385 layers can be in Figure 6. The sol-gel sealers showed an increase in
 386 impedance, compared to the PAA blank, in the high frequency range
 387 (~1 × 10⁶ Hz). As the pores of PAA anodic layers are known to remain
 388 open indefinitely¹ the encapsulation of the sol-gel sealers results in
 389 this increase in the impedance compared to the PAA blank. In contrast
 390 to the SAA PhTEOS layer the PAA PhTEOS layer exhibits a two time
 391 constant response. The barrier layer of the PAA anodic layer will be
 392 thicker, due to higher forming voltage than the SAA equivalent, and
 393 perhaps this increased oxide thickness results in the discrimination
 394 between the sol-gel material and the anodic alumina barrier layer.
 395 The low frequency impedance of the PAA Si-Zr layer exhibits lower
 396 impedance values than the PhTEOS equivalent. The low frequency
 397 impedance (0.1 Hz) of the PAA Si-Zr is equivalent to the PAA blank.
 398 The PhTEOS sealer shows higher impedance than both the PAA blank
 399 and the PAA Si-Zr sample. This may be due to better penetration of
 400 the PhTEOS sol-gel to the base of the pores to the barrier layer.

401 The impedance and phase shift spectra for DA sealed anodic lay-
 402 ers can be seen in Figure 7. The DA HTS samples exhibits a similar
 403 response to the SAA HTS sample with a single time constant de-
 404 tected. Significantly, despite the increased thickness of the SAA layer
 405 compared to the sulphuric acid formed layer in the DA structure the
 406 impedance response are relatively similar. The EIS response in both

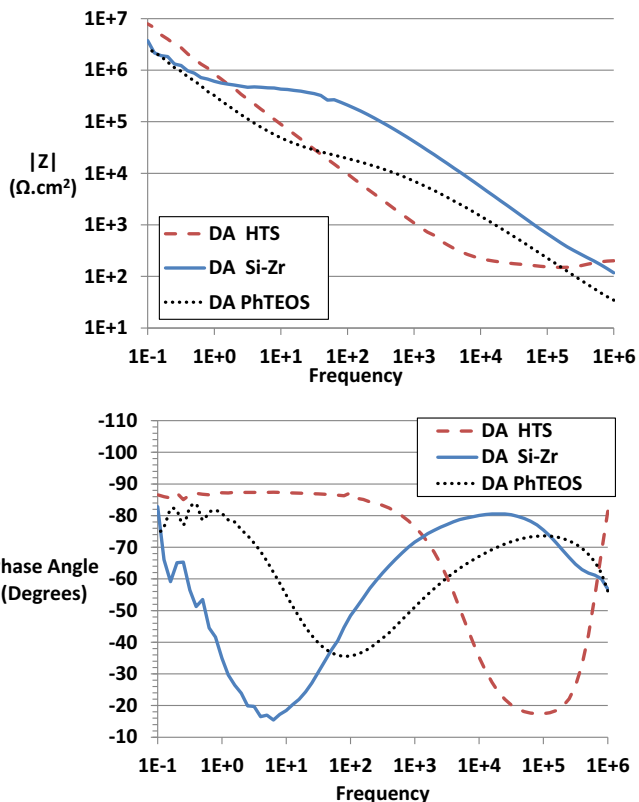


Figure 7. Impedance (top) and phase plot (bottom) for DA sealed samples.

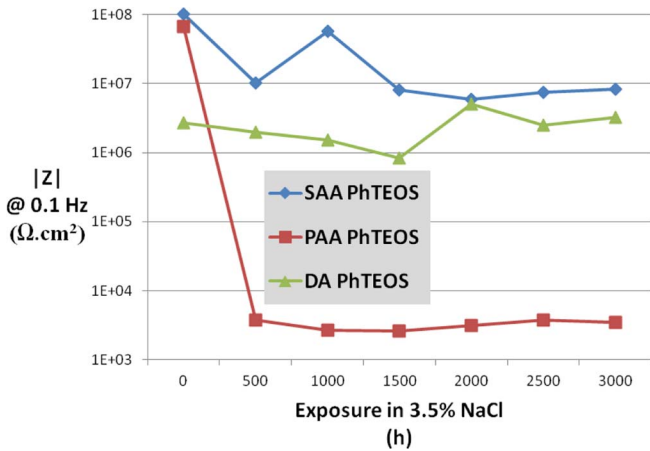


Figure 8. Plot of impedance as a function of time for PhTEOS treated layers exposed to 3.5% NaCl.

cases is from the barrier layer only.³⁷ For both of the sol-gel sealers the low frequency impedance (0.1 Hz) is lower than the DA HTS. This indicates, as expected, that the sealing effect has not progressed into the nanoporous structure and influenced the barrier layer properties. The presence of the sol-gel sealers may also have prevented any natural hydration which proceeds after the hydrothermal treatment as the sol-gels area applied almost immediately after hydrothermal sealing. This may explain the elevated low frequency impedance levels of the DA HTS compared to the sol-gel sealed equivalents. In the mid to high frequency range (>100 Hz) the sol-gel sealers show elevated impedance levels, compared to the DA HTS sample. The first time constant for the sol-gel sealers, appearing in the high frequency end of the spectrum, is as a result the sol-gel/oxide composite layer formed on the surface of the sample. The second time constant is the barrier layer contribution.

By plotting the impedance at 0.1 Hz over time the evolution of barrier properties can be determined for each sol-gel sealer. The protection properties of the PhTEOS sealed anodic layers during continuous exposure to the 3.5% NaCl solution can be seen in Figure 8. For the PhTEOS sealed anodic layers the SAA and DA layers appear relatively stable with a small gradual decrease up to 1500 h. The impedance of the PAA layer drops rapidly between 0 and 500 h exposure. At this exposure time the PAA PhTEOS sealed layer exhibits extensive pitting and corrosion. The increased impedance of the SAA system compared to the DA is likely due to the longer anodising duration of the SAA system. Interestingly at 1500–2000 h both the SAA and DA PhTEOS sealed surfaces begin to increase marginally in impedance. The rapid deterioration of the PAA layer, despite achieving full encapsulation indicates the importance of the presence of an anodic layer that has the ability to seal naturally.

Again the evolution of the Si-Zr sealed anodic layers can be seen by plotting the low frequency impedance over exposure duration as

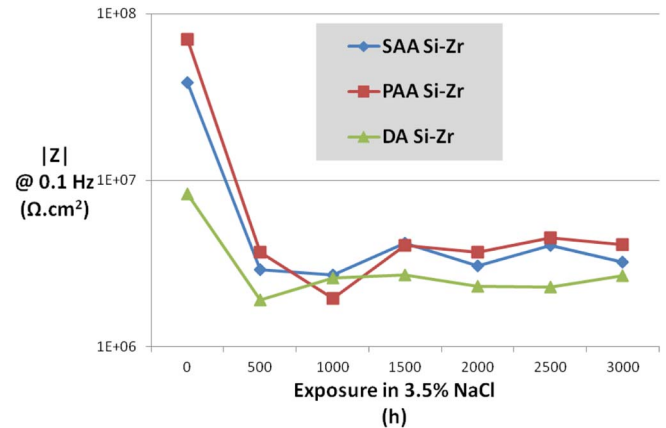


Figure 9. Plot of impedance as a function of time for Si-Zr treated layers exposed to 3.5% NaCl.

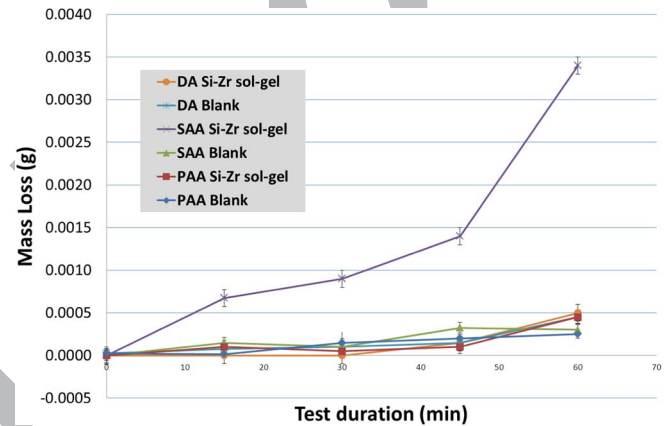


Figure 10. Rain erosion performance of anodised and sol-gel sealed systems on clad 2024-T3.

seen in Figure 9. The Si-Zr sol-gel sealed anodic layers all experience an impedance drop of approximately one order of magnitude after 500 h. This initial drop is possibly due to uptake of electrolyte by the sol-gel coating. After this time the impedance of all the surfaces stabilise and remain consistent up to 3000 h exposure with no pitting or corrosion evident on the surfaces.

With the exception of the PhTEOS sealed PAA layer the anodised AA2024 surfaces appear stable up to 3000 h exposure. This is a significant duration for immersion in a chloride rich solution without a considerable loss in barrier properties.

Neutral salt spray.—Neutral salt spray exposure was also conducted on the anodised and sol-gel sealed samples and a corrosion rating has been assigned as per Table I. Unsealed equivalents have

Table I. Neutral salt spray corrosion ratings of anodic layers on AA2024-T3.

Treatment		First Cor TCorr ₀	NSS Duration							
Anodising	Sol-gel		24 h	168 h	500 h	750 h	1000 h	1500 h	2000 h	3500 h
SAA	BLANK	24	1	6	50	50	-	-	-	-
PAA	BLANK	24	200	-	-	-	-	-	-	-
DA	BLANK	72	0	12	200	-	-	-	-	-
SAA	PhTEOS	24	1	12	50	100	-	-	-	-
PAA	PhTEOS	24	50	200	-	-	-	-	-	-
DA	PhTEOS	500	0	0	1	12	12	25	-	-
SAA	Si-Zr	3500	0	0	0	0	0	0	0	1
PAA	Si-Zr	500	0	0	1	12	25	200	-	-
DA	Si-Zr	1000	0	0	0	0	1	6	-	-

452 been used for comparison. As expected in the unsealed form, the
 453 SAA, PAA and DA surfaces offer little protection with corrosion oc-
 454 ccurring rapidly. The SAA and PAA layers exhibited pitting corrosion
 455 after 24 h exposure with the DA surface remaining clear of corro-
 456 sion until 72 h exposure. Upon the onset of initial corrosion, pitting
 457 increases rapidly for all of the unsealed anodised surfaces. The pres-
 458 ence of the sol-gel within the pores of the SAA layer appears to have a
 459 negative effect on corrosion prevention with a marginally higher level
 460 of pitting exhibited on the PhTEOS treated surface when compared
 461 to the unsealed SAA. This is possibly due to the effect on hydration
 462 due to the presence of the sol-gel within the aluminum oxide network.
 463 The sol-gel may retard the hydration of the surfaces as has been
 464 previously reported.⁹ In the case of the PhTEOS PAA layer there is
 465 a marginal reduction in pitting however the improvement over the
 466 unsealed PAA is negligible. The PhTEOS sealed DA layer exhibited
 467 a marked increase in pitting prevention over the other PhTEOS sealed
 468 anodised finishes. This displays the value in utilising the DA process,
 469 as the natural hydration properties of the anodic layers are retained,
 470 while the sol-gel is also encapsulated in aluminum oxide.

471 The negative effect of the PhTEOS sealer on the SAA layer during
 472 neutral salt spray was not identified by the EIS analysis. One possible
 473 explanation is the difference in exposure area during the test. The
 474 much larger surface area exposed during the NSS test may be more
 475 indicative of the actual corrosion resistance than the smaller area EIS.
 476 For all samples the discrimination in corrosion resistance is greater by
 477 NSS than EIS indicating that the NSS is possibly a more aggressive
 478 test. The authors also believe that the EIS immersion cycle allows the
 479 natural hydration of the layers to proceed better than the salt fog test.
 480 Additionally, the salt fog test has reported to delaminate and remove
 481 sol-gel coatings attached to anodic layers,²⁷ which may result in a
 482 more aggressive corrosion effect.

483 The Si-Zr sol-gel displays enhanced pitting corrosion protection
 484 over the PhTEOS sol-gel sealed systems. The increased barrier prop-
 485 erties as well as the inclusion of an active corrosion inhibitor results
 486 in a significant level of protection for all anodising treatments. The
 487 SAA layer in particular exhibits remarkable corrosion resistance with
 488 no evidence of pitting at 3500 h. The absence of pore penetration of
 489 the Si-Zr sol ensures that the natural hydration properties of the SAA
 490 layer are retained unlike the PhTEOS equivalent. Furthermore, the
 491 inclusion of an the tetrazine based corrosion inhibitor may also have
 492 a positive effect on the integrity of the SAA layer as tetrazines are
 493 known to bind to and chelate copper ions.³⁸ These inhibitors have been
 494 studied as standalone treatments for anodic layers and have shown in-
 495 creased ability to inhibit pitting corrosion.³⁸ The DA equivalent shows
 496 a higher degree of degradation, when compared to the SAA equiv-
 497 alent, possibly due to the decreased thickness of the SAA layer. The
 498 worst performing Si-Zr sealed layer is the PAA.

499 **Rain erosion.**—Anodising is often used to increase the surface
 500 hardness and abrasion resistance of aluminum alloys.¹ By incorpo-
 501 rating the sol-gel coating into the aluminum oxide network elevated
 502 mechanical properties are afforded to the sol-gel coating. This will
 503 improve the hardness, abrasion resistance and impact resistance of
 504 the sol-gel coatings. A significant advantage of increased mechanical
 505 performance for the aerospace industry is the decreased effect of rain
 506 erosion. Erosion of aerospace grade aluminum alloys by impinging
 507 water droplets is a significant issue especially during aircraft take-off
 508 and landing.^{39,40}

509 Whirling arm rain erosion evaluation of the Si-Zr sol-gel sealed
 510 clad 2024-T3 samples was conducted and the weight loss over the 60
 511 min exposure was recorded as seen in Figure 9. The weight loss for
 512 the sol-gel applied on the SAA is significantly greater than any other
 513 surface tested. From the EDX analysis (Figure 4), it is determined
 514 that the sol-gel forms a surface coating on the SAA surface with
 515 limited encapsulation in the porous anodic alumina. Therefore, the
 516 rain erosion and weight loss of this system is of the sol-gel coating
 517 only, which is mechanically inferior to the aluminum oxides produced
 518 from SAA, PAA and DA as well as the sol-gel/alumina composites
 519 produced from sol-gel encapsulation.

This indicates that the encapsulation of the sol-gel coatings in
 anodic alumina presents a significant improvement in rain erosion.
 The weight loss of the bare anodic layers or sol-gel encapsulated
 layers is minimal.

Sol-gel materials have been studied extensively for replacement
 of chromate materials as they can act as reservoirs for active corro-
 sion inhibitors. However for many sol-gel coating additives there is a
 critical concentration after which the additive affects the film forming
 properties and integrity of the applied sol-gel film. Excess amounts
 of corrosion inhibitors have shown to have a negative effect on film
 forming properties of sol-gel coatings.⁴¹⁻⁴³ By utilising a duplex an-
 odic oxide, the active corrosion inhibitors can be incorporated in the
 SAA layer at a significantly higher concentration while the sol-gel
 can be encapsulated in the porous PAA network. As shown from the
 results, the DA layer is particularly suitable for sol-gel sealing. Due
 to the low thickness of sol-gel coatings, the PAA layer can be tailored
 to result in full encapsulation of the sol-gel coating within the anodic
 structure. Furthermore, conventional sealing methods can be applied
 to the SAA base layer of the DA structure. This results in elevated
 corrosion resistance while also preventing the sol-gel material from
 migrating into the SAA pores. This becomes particularly important
 with clad AA2024 or non copper containing alloys as the natural
 hydration properties of SAA layer is therefore not affected by the
 presence of the sol-gel material. The DA process developed can also
 be utilised for adhesion and bonding applications while also retaining
 a significant level of corrosion resistance on aluminum alloys.

Conclusions

Duplex anodic layers have been developed to achieve sol-gel en-
 capsulation in porous anodic alumina to ensure that the natural hydra-
 tion properties of anodised aluminum is retained. By encapsulating
 sol-gel materials in phosphoric acid anodised aluminum the mechan-
 ical properties of the sol-gel coatings are enhanced. By forming a
 sulphuric acid anodised layer between the sol-gel/oxide composite
 and the substrate the combined corrosion resistance is significantly
 enhanced. The value of utilising the duplex anodic layers is evident
 due to the achievable anti-corrosion performance on corrosion prone
 2024-T3, sealed with a simple organically modified silane based sol-
 gel. The performance is further enhanced by applying a Si-Zr hybrid
 sol-gel with active tetrazine based inhibitor. For all systems the ab-
 sence of the sol-gel from the pores of the SAA layers is critical to
 allow the natural or accelerated hydration of the systems to proceed.

Acknowledgments

This work is supported by Enterprise Ireland under the Technol-
 ogy Gateway Programme and the European Union under the Seventh
 Framework Programme, project 266029 “Aeromuco”.

References

1. S. Wernick, R. Pinner, and P. G. Sheasby, *The Surface Treatment and Finishing of Aluminum and its Alloys*, 5th ed., Finishing Publications Ltd. 1987.
2. V. F. Henley, *Anodic Oxidation of Aluminium & its Alloys*, Pergamon Press 1982.
3. S. J. Garcia-Vergara, L. Iglesias-Rubianes, C. E. Blanco-Pinzon, P. Skeldon, G. E. Thompson, and P. Campestrini, “Mechanical instability and pore generation in anodic alumina,” *Proceedings of the Royal Society A: Mathematical, Physical and Engineering Science*, **462**, 2345 (2006).
4. S. J. Garcia-Vergara, P. Skeldon, G. E. Thompson, and H. Habazaki, “Stress generated porosity in anodic alumina formed in sulphuric acid electrolyte,” *Corrosion Science*, **49**, 3772 (2007).
5. S. J. Garcia-Vergara, P. Skeldon, G. E. Thompson, T. Hashimoto, and H. Habazaki, “Compositional Evidence for Flow in Anodic Films on Aluminum under High Electric Fields,” *Journal of The Electrochemical Society*, **154**, C540 (2007).
6. S. J. Garcia-Vergara, P. Skeldon, G. E. Thompson, and H. Habazaki, “Tracer studies of anodic films formed on aluminum in malonic and oxalic acids,” *Applied Surface Science*, **254**, 1534 (2007).
7. J. A. González, M. Morcillo, E. Escudero, V. López, and E. Otero, “Atmospheric corrosion of bare and anodized aluminum in a wide range of environmental conditions. Part I: Visual observations and gravimetric results,” *Surf. Coat. Technol.*, **153**, 225 (2002).

- 585 8. J. A. Gonzalez, M. Morcillo, E. Escudero, V. Lopez, A. Bautista, and E. Otero, 634
586 Self-sealing of unsealed aluminum anodic oxide films in very different atmospheres, 635
587 *Revista de Metalurgia, Extr CODEN RMTGAC* (2003) 110. 636
- 588 9. M. Whelan, J. Cassidy, and B. Duffy, "Sol-gel sealing characteristics for corrosion 637
589 resistance of anodised aluminum," *Surf. Coat. Technol.*, **235**, 86 (2013). 638
- 590 10. M. J. Bartolomé, J. F. del Río, E. Escudero, S. Feliu Jr, V. López, E. Otero, and 639
591 J. A. González, "Behaviour of different bare and anodised aluminum alloys in the 640
592 atmosphere," *Surf. Coat. Technol.*, **202**, 2783 (2008). 641
- 593 11. E. Escudero, V. López, E. Otero, M. J. Bartolomé, and J. A. González, "Behaviour of 642
594 anodised aluminum in very long-term atmospheric exposure," *Surf. Coat. Technol.*, 643
595 **201**, 7303 (2007). 644
- 596 12. T. Hashimoto, X. Zhou, P. Skeldon, and G. E. Thompson, "Structure of the Copper- 645
597 Enriched Layer Introduced by Anodic Oxidation of Copper-Containing Aluminium 646
598 Alloy," *Electrochim. Acta*, **179** 394. 647
- 599 13. L. Domingues, J. C. S. Fernandes, M. Da Cunha Belo, M. G. S. Ferreira, and 648
600 L. Guerra-Rosa, "Anodising of Al 2024-T3 in a modified sulphuric acid/boric acid 649
601 bath for aeronautical applications," *Corros. Sci.*, **45**, 149 (2003). 650
- 602 14. M. A. Arenas, A. Conde, and J. J. de Damborenea, "Effect of acid traces on hydro- 651
603 thermal sealing of anodising layers on 2024 aluminum alloy," *Electrochim. Acta*, 652
604 **55**, 8704 (2010). 653
- 605 15. P. C. R. Varma, J. Colreavy, J. Cassidy, M. Oubaha, B. Duffy, and C. McDonagh, 654
606 "Effect of organic chelates on the performance of hybrid sol-gel coated AA 2024-T3 655
607 aluminum alloys," *Prog. Org. Coat.*, **66**, 406 (2009). 656
- 608 16. P. C. R. Varma, P. Periyat, M. Oubaha, C. McDonagh, and B. Duffy, "Application 657
609 of niobium enriched ormosils as thermally stable coatings for aerospace aluminum 658
610 alloys," *Surf. Coat. Technol.*, **205**, 3992 (2011). 659
- 611 17. R. V. Padinchare Covilakath, J. Cassidy, M. Oubaha, C. McDonagh, J. Colreavy, 660
612 and B. Duffy, "Corrosion Protection Properties of Various Ligand Modified Organic 661
613 Inorganic Hybrid Coating on AA 2024-T3," *ECS Transactions*, **24**, 231 662
614 (2010). 663
- 615 18. J. Livage, M. Henry, and C. Sanchez, "Sol-gel chemistry of transition metal oxides," 664
616 *Progress in Solid State Chemistry*, **18**, 259 (1988). 665
- 617 19. G. S. C. J. Brinker, *Sol-Gel Science: The Physics and Chemistry of Sol-Gel Process-* 666
618 *ing*, Academic Press, San Diego, CA, 1990. 667
- 619 20. L. L. Hench and J. K. West, "The sol-gel process," *Chemical Reviews*, **90**, 33 668
620 (1990). 669
- 621 21. M. L. Zheludkevich, I. M. Salvado, and M. G. S. Ferreira, "Sol-gel coatings for cor- 670
622 rosion protection of metals," *Journal of Materials Chemistry*, **15**, 5099 (2005). 671
- 623 22. M. Guglielmi, "Sol-gel coatings on metals," *Journal of Sol-Gel Science and Tech-* 672
624 *nology*, **8**, 443 (1997). 673
- 625 23. C. Sanchez, B. Julian, P. Belleville, and M. Popall, "Applications of hybrid organic- 674
626 inorganic nanocomposites," *Journal of Materials Chemistry*, **15**, 3559 (2005). 675
- 627 24. P. G.-R. C. Sanchez and Functional Hybrid Materials 2004. 676
- 628 25. R. L. Parkhill, E. T. Knobbe, and M. S. Donley, "Application and evaluation of envi- 677
629 ronmentally compliant spray-coated ormosil films as corrosion resistant treatments 678
630 for aluminum 2024-T3," *Progress in Organic Coatings*, **41**, 261 (2001). 679
- 631 26. M. Whelan, J. Cassidy, and B. Duffy, "Sol-gel Sealing Characteristics for Corrosion 680
632 Resistance of Anodised Aluminium," *Surface and Coatings Technology* (2013), doi: 681
633 10.1016/j.surfcoat.2013.07.018. 682
27. V. R. Capelossi, M. Poelman, I. Recloux, R. P. B. Hernandez, H. G. de Melo, and 634
635 M. G. Olivier, "Corrosion protection of clad 2024 aluminum alloy anodized in 636
637 tartaric-sulfuric acid bath and protected with hybrid sol-gel coating," *Electrochim.* 638
639 *Acta*, **124**, 69 (2014). 640
- 641 28. G. W. Critchlow, K. A. Yendall, T. Cartwright, and I. A. Ashcroft, "Environmentally- 642
643 friendly surface treatments, Automotive Adhesives, Sealants & Coatings," *Proceed-* 644
645 *ings of the Conference*, Rapra Smithers, Stuttgart, Germany, 2008, pp. 18/11-18/11. 646
- 647 29. J. Colreavy, B. Duffy, P. C. R. Varma, H. Hayden, and O. Mohamed, Sol-Gel Coating 648
649 Compositions and their Process of Preparation, EP2220176 (2010). 650
- 651 30. M. García-Rubio, M. P. de Lara, P. Ocón, S. Diekhoff, M. Beneke, A. Lavía, and 652
653 I. García, "Effect of posttreatment on the corrosion behaviour of tartaric sulphuric 654
655 anodic films," *Electrochim. Acta*, **54**, 4789 (2009). 656
- 657 31. V. Moutarlier, M. P. Gigandet, J. Pagetti, and L. Ricq, "Molybdate/sulfuric acid an- 658
659 odising of 2024-aluminum alloy: influence of inhibitor concentration on film growth 659
660 and on corrosion resistance," *Surf. Coat. Technol.*, **173**, 87 (2003). 661
- 662 32. O. Zubillaga, F. J. Cano, I. Azkarate, I. S. Molchan, G. E. Thompson, and P. Skeldon, 663
664 "Synthesis of anodic films in the presence of aniline and TiO₂ nanoparticles on 664
665 AA2024-T3 aluminum alloy," *Thin Solid Films*, **517**, 6742 (2009). 666
- 667 33. M. García-Rubio, P. Ocón, M. Curioni, G. E. Thompson, P. Skeldon, A. Lavía, and 668
669 I. García, "Degradation of the corrosion resistance of anodic oxide films through 669
670 immersion in the anodising electrolyte," *Corros. Sci.*, **52**, 2219 (2010). 670
- 671 34. K. Shimizu, H. Habazaki, P. Skeldon, G. E. Thompson, and G. C. Wood, "Migration 671
672 of oxalate ions in anodic alumina," *Electrochim. Acta*, **46**, 4379 (2001). 672
- 673 35. K. Shimizu, H. Habazaki, P. Skeldon, G. E. Thompson, and G. C. Wood, "Migration 673
674 of sulfate ions in anodic alumina," *Electrochim. Acta*, **45**, 1805 (2000). 674
- 675 36. A. Santos, L. Vojkuvka, J. Pallarés, J. Ferré-Borrull, and L. F. Marsal, "In situ elec- 675
676 trochemical dissolution of the oxide barrier layer of porous anodic alumina fabricated 676
677 by hard anodization," *J. Electroanal. Chem.*, **632**, 139 (2009). 677
- 678 37. M. Franco, S. Anoop, R. Uma Rani, and A. K. Sharma, Porous Layer Characterization 678
679 of Anodized and Black-Anodized Aluminium by Electrochemical Studies, ISRN 679
680 Corrosion, 2012 Article ID 323676 (2012) 12. 680
- 681 38. M. Whelan, K. Barton, J. Cassidy, J. Colreavy, and B. Duffy, "Corrosion inhibitors 681
682 for anodised aluminum," *Surf. Coat. Technol.*, **227**, 75 (2013). 682
- 683 39. P. Lammel, L. D. Rafailovic, M. Kolb, K. Pohl, A. H. Whitehead, G. Grundmeier, 683
684 and B. Gollas, "Analysis of rain erosion resistance of electroplated nickel-tungsten 684
685 alloy coatings," *Surf. Coat. Technol.*, **206**, 2545 (2012). 685
- 686 40. E. F. Tobin, T. M. Young, D. Raps, and O. Rohr, "Comparison of liquid impingement 686
687 results from whirling arm and water-jet rain erosion test facilities," *Wear*, **271**, 2625 687
688 (2011). 688
- 689 41. P. C. R. Varma, B. Duffy, and J. Cassidy, "Influence of magnesium nitrate on the 689
690 corrosion performance of sol-gel coated AA2024-T3 aluminum alloy," *Surf. Coat.* 689
691 *Technol.*, **204**, 277 (2009). 690
- 692 42. J. H. Osborne, K. Y. Blohowiak, S. R. Taylor, C. Hunter, G. Bierwagon, B. Carlson, 691
693 D. Bernard, and M. S. Donley, "Testing and evaluation of anodic of nonchromated coating 692
694 systems for aerospace applications," *Prog. Org. Coat.*, **41**, 217 (2001). 693
- 695 43. M. Schem, T. Schmidt, J. Gerwamm, M. Wittmar, M. Veith, G. E. Thompson, 694
696 I. S. Molchan, T. Hashimoto, P. Skeldon, A. R. Phani, S. Santucci, and 695
697 M. L. Zheludkevich, "CeO₂-filled sol-gel coatings for corrosion protection of 696
698 AA2024-T3 aluminum alloy," *Corros. Sci.*, **51**, 2304 (2009). 697
698

Queries

Q1: AU: Please provide text citation for Fig. 10.

Q2: AU: Please provide a digital object identifier (doi) for Ref(s) 22. For additional information on doi's please select this link: <http://www.doi.org/>. If a doi is not available, no other information is needed from you.